

Polydisperse polymer fractionation between phases

J. Pedro de Souza,^{*,†} William M. Jacobs,^{*,‡} and Howard A. Stone^{*,¶}

[†]*Omenn-Darling Bioengineering Institute, Princeton University, Princeton, NJ, 08544*

[‡]*Department of Chemistry, Princeton University, Princeton, NJ 08544, USA.*

[¶]*Department of Mechanical and Aerospace Engineering, Princeton University, Princeton, NJ, 08544*

E-mail: pdesouza@princeton.edu; wjacobs@princeton.edu; hastone@princeton.edu

Abstract

Polymer mixtures fractionate between phases depending on their molecular weight. Consequently, by varying solvent conditions, a polydisperse polymer sample can be separated between phases so as to achieve a particular molecular weight distribution in each phase. In principle, predictive physics-based theories can help guide separation design and interpret experimental fractionation measurements. Even so, applying the standard Flory-Huggins model can present a computational challenge for mixtures with many polymeric components of different length, particularly for scarce components at the tails of a distribution. Here, we apply our recently-derived exact analytical solution of multi-component Flory-Huggins theory for polydisperse polymers to understand the principles of polymer fractionation for common molecular weight distributions. Our method reveals that polymer fractionation is highly sensitive to the shape, and in particular the tails, of this distribution. Our results highlight the need for considering the full molecular weight distribution in phase coexistence calculations.

The fractionation of polymers refers to the re-distribution of polymers of different types and/or lengths between phases.¹⁻³ The simplest scenario is when all polymers are chemically identical in their monomer composition, but differ in their length or molecular weight (MW), which is called polydispersity.^{4,5} Virtually all polymer samples exhibit some degree of polydispersity arising from their synthesis conditions.⁶⁻⁸

If placed in a poor solvent, the polydisperse polymer will phase separate into a condensed (concentrated) polymer phase and a dilute phase composed primarily of solvent. The two phases will differ in their MW distributions,⁹ since the entropy of demixing differs based on polymer length. As an example, a polydisperse polymer sample separates into a dilute phase, which is enriched in shorter polymers, and a concentrated phase, which is enriched in longer polymers, as illustrated in Figure 1.

From synthetic to naturally occurring polymers, the MW polydispersity depends on poly-

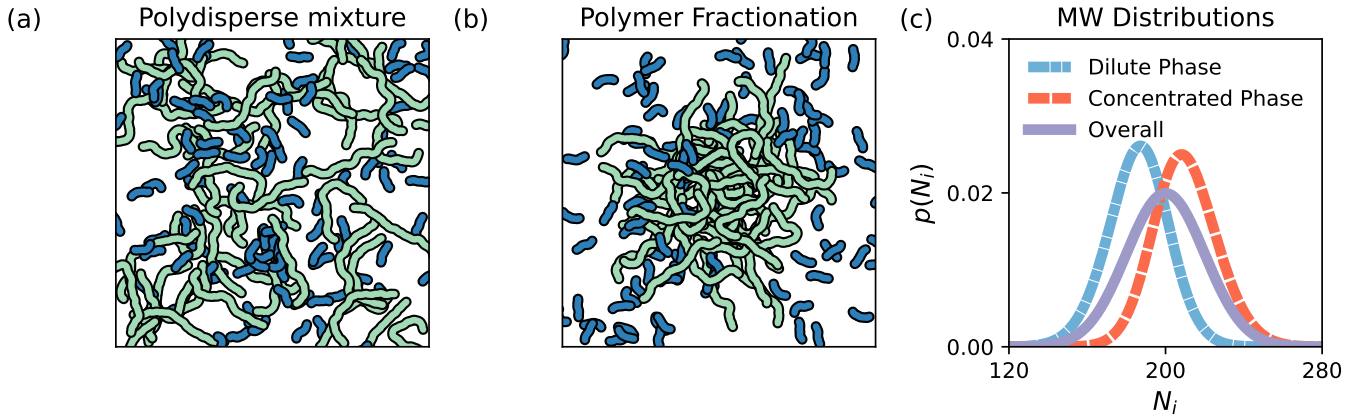


Figure 1: Polymer fractionation between phases. (a) A uniformly mixed polydisperse sample of long polymers (green) and short polymers (blue). (b) When this polydisperse mixture phase separates, longer polymers are preferentially concentrated in the concentrated phase and shorter polymers are preferentially accumulated in the dilute phase. (c) Generic fractionation behavior. The purple curve corresponds to the overall MW distribution of a “dry” polymer sample exhibiting a normal distribution, the blue corresponds to the dilute B phase, and the red corresponds to the concentrated A phase when the polymer is placed in solvent. The MW distributions are expressed as a mass fraction probability density, $p(N_i)$, where N_i is the number of monomers in component i , computed for a particular interaction strength and condensed volume fraction.

merization reaction conditions and the degree of homogeneity of a sample. For example, “living” polymers, which are formed by monomer addition without termination, follow a modified Poisson distribution.^{1,4} The Flory-Schulz distribution, which exhibits an extended tail, is frequently observed for linear polymers synthesized by step-growth reactions. Polymers synthesized by chain growth reactions have more diverse MW distributions,⁶ which can be generically fit to normal or log-normal distributions.¹⁰ On the other hand, naturally occurring biopolymers such as RNA and proteins have precisely defined MWs dependent on their sequence definition, yet they exist in complex polydisperse biological mixtures. The four common MW distributions that we study are given in Table 1.

In industrial applications, a particular polymer MW distribution is needed to create materials of desired mechanical,¹¹ rheological,¹² thermal¹³ and thermoresponsive,¹⁴ electrical,¹⁵ or optical¹⁶ properties.^{5,8} Thus, by carefully choosing a solvent and/or processing temperature, polymer fractionation may be a simple route to concentrate particular polymer MWs into either a condensed or dilute phase. Similarly, naturally occurring biopolymers within cells may be fractionated between condensed and dilute phases by forming biomolecular condensates.^{17–19} For example, certain RNA granules exhibit a higher propensity to concentrate longer RNA with more exposed sequences.²⁰

Table 1: The MW distributions studied in this work, expressed as a mass fraction of polymer chains of length N_i . For the normal distribution, $\langle N \rangle$ describes the center of the distribution, while N_σ describes the standard deviation. In the modified-Poisson distribution, the λ parameter encapsulates both the average and variance of the distribution. For the bimodal distribution, the parameters N_1 and N_2 characterize the centers of the peaks in the MW distribution, while N_σ describes the standard deviation. The parameter b describes the extent of reaction $0 < b < 1$ for Flory-Schulz.

MW Distribution	Normal Distribution	Modified Poisson	Bimodal	Flory-Schulz
$p(N_i)$	$\frac{\exp\left(-\frac{(N_i - \langle N \rangle)^2}{2N_\sigma^2}\right)}{\sqrt{2\pi N_\sigma^2}}$	$\frac{\lambda}{\lambda+1} \frac{N_i e^{-\lambda} \lambda^{N_i-2}}{(N_i-1)!}$	$f p_{\text{norm}}(N_i, N_1, N_\sigma) + (1-f) p_{\text{norm}}(N_i, N_2, N_\sigma)$	$N_i(1-b)^2 b^{N_i-1}$
Weight Average $\langle N \rangle$	$\langle N \rangle$	$\lambda + 2 - \frac{1}{\lambda+1}$	$f N_1 + (1-f) N_2$	$\frac{1+b}{1-b}$

Theoretical model predictions of polymer fractionation explain phase behavior at a quantitative level and aid in process design. Even so, phase coexistence calculations are computationally demanding,^{19,21,22} especially for large numbers of discrete MWs or when certain components are present in minute quantities in the tails of the MW distribution. In our recent work,²³ we found an exact implicit analytical solution to two-phase coexistence within the Flory-Huggins model describing a polydisperse polymer mixture with any number of components. The exact solution allows us to evaluate the interplay of polydispersity and phase separation at high numerical accuracy. Further, we can self-consistently predict the fractionation of polymers between phases over the entire phase diagram with minimal computational effort.

Here, we explore the effects of polydispersity for common MW distributions, employing our analytical method that simply requires evaluating a set of analytical formulas. We find that the extent of polydispersity, along with the tails of the distribution, can strongly influence the phase diagram and resulting fractionation between phases. The approaches presented here may allow for an interpretation of the phase behavior of polymer samples including consideration of a realistic distribution of MWs. Further, our analysis may be useful for designing a polymer fractionation process by varying solvent conditions.

Within the framework of Flory-Huggins theory, we assume that the enthalpic interactions between monomers are the same regardless of polymer chain length. The free energy density, f , of polydisperse polymers of length N_i , filling a lattice with volume v per monomer or solvent molecule, is

$$\frac{fv}{k_B T} = \sum_i \frac{1}{N_i} \phi_i \ln(\phi_i) + (1 - \phi_t) \ln(1 - \phi_t) - \chi \phi_t^2, \quad (1)$$

where ϕ_i is the volume fraction of component i , $\phi_t = \sum_i \phi_i$ is the total polymer volume fraction, and χ represents the interactions of the polymer with itself and with the solvent. The summation over i accounts for all M polymeric components of differing lengths.

Here, we will assume that phase separation results in coexistence between two phases. At thermodynamic equilibrium, each component i must have equal chemical potential, μ_i , in each phase, and the osmotic pressure, Π , between phases A (condensed) and B (dilute) must be identical,

$$\mu_i(\Phi_A) = \mu_i(\Phi_B) \quad (2a)$$

$$\Pi(\Phi_A) = \Pi(\Phi_B), \quad (2b)$$

where Φ is a vector containing the volume fractions of each component i . The chemical potential is derived as

$$\frac{\mu_i}{k_B T} = \frac{1}{N_i} \ln(\phi_i) - \ln(1 - \phi_t) - 2\chi\phi_t, \quad (3)$$

and the osmotic pressure is

$$\frac{\Pi v}{k_B T} = -\ln(1 - \phi_t) - \chi\phi_t^2 - \phi_t + \sum_i \frac{\phi_i}{N_i}. \quad (4)$$

Along with mass balances between the phases for each component i (SI Section S2) and equations (2a) and (2b), we have a nonlinear system of equations that scales with the number of components. However, this system is difficult to solve directly. Flory¹ and Huggins²⁴ each noted that the chemical equilibrium, by equating $\mu_i - \Pi$ (in our notation) for each specie, directly gives a relationship describing the fractionation of each polymer up to an undetermined parameter which was fitted to experimental data at each condition (SI Section S1). Yet, the approach does not provide an exact solution for phase coexistence, and Flory even stated that “A complete calculation of the phase equilibrium from the equations would be a staggering task”.¹ Therefore, the approach may be useful for data interpretation, but is not directly predictive or transferable between different experimental conditions.

In this work, we employ an implicit substitution method to solve the two-phase coexistence problem exactly, and we refer an interested reader to SI Section S2 for specific details about the calculation. The key idea is that we treat the value of χ implicitly, inverting

the problem into one transcendental equation in one unknown composite variable, and then transforming back to real compositions. We highlight that Flory’s note about the exact solution rings true—the method is algebraically involved, requiring mappings between composition coordinates, but nevertheless is computationally efficient to generate the thermodynamic coexistence curves by direct evaluation of analytical formulas. The exact solution is also advantageous since the computations can be done with high numerical accuracy, a feature that may be difficult to implement with other approaches. We will demonstrate that this accuracy is important since subtle features of MW distributions can have a strong influence on the phase diagram.

The results are organized as follows. Using our analytical method, we first evaluate the fractionation of different distributions near the cloud point—defined as the point when an infinitesimal amount of condensed phase forms. We then examine how the distribution can influence the observed phase diagram, which is typically measured at the cloud point. Finally, we calculate complete phase diagrams for polydisperse samples over the full polymer/solvent composition range to identify how the phase coexistence shifts as the condensed phase volume changes.

In Fig. 2 we calculate the MW distribution in the condensed phase at the cloud point with $\chi = 0.8$ for the four different distributions listed in Table 1. At the cloud point, the overall distribution of the polymer sample (purple) matches the distribution in the dilute phase, but differs from the condensed phase (red). The parameterizations of the overall distributions are chosen such that the weight average chain length, $\langle N \rangle$, is ≈ 200 for at least one of the curves from each distribution ($\langle N \rangle = 200$ in (a), $\lambda = 200$ in (b), $f = 0.5$ in (c) and $b=0.99$ in (d)). These curves at constant $\langle N \rangle$ can be compared directly to examine the effect of the MW distribution.

First, in Fig. 2(a), by comparing normally-distributed samples of different standard deviation, N_σ , but with the same mean, $\langle N \rangle$, we demonstrate that greater polydispersity leads to greater fractionation from the high MW tails of the distribution. Therefore, the

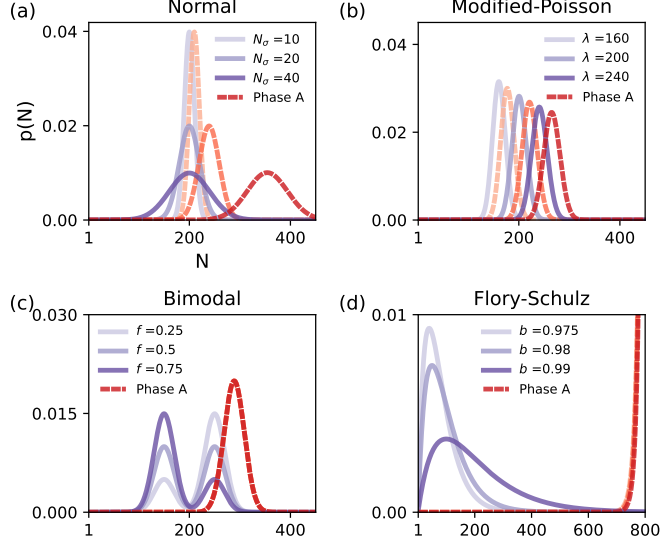


Figure 2: Fractionation at the cloud point. The MW distributions with $\chi = 0.8$ at the cloud point, when the condensed phase (Phase A) first appears. The shade of the line designates a correspondence between the overall distribution (purple) and the condensed distribution (red). The distributions tested are (a) normal distribution centered at $N_1 = 200$ with varying standard deviation, N_σ , (b) modified-Poisson distributions with varying λ parameters, (c) bimodal distributions with $N_2 = 250$ and $N_1 = 150$ with $N_\sigma = 20$, varying the fraction f of the first peak, and (d) Flory-Schulz for varying degrees of polymerization, b . More polydisperse samples exhibit greater fractionation, and the fractionation is dominated by the tails of the distribution.

condensed phase from a sample with greater variance will have a greater mean MW.

In contrast, the modified Poisson distribution in Fig. 2(b) exhibits sharper, more uniform peaks than the other distributions.²⁵ There is relatively small translation in the MW distribution in the condensed phase relative to the overall distribution, although this translation increases with increasing value of λ .

The role of the highest peak in the overall MW distribution is clearly apparent for the bimodal distribution shown in Fig. 2(c). No matter the ratio of the two peaks in the bimodal distribution, the MW distribution in the condensed phase is nearly identical and centered on the right arm of the higher MW peak.

The Flory-Schulz distribution, shown in Fig. 1(d), is unique from the other distributions studied here in that the tail decays slower than exponentially. As a result, the fractionation

at the cloud point is dominated by the longest polymer included in the sample, as we prove mathematically in the SI Section S3. For our sample calculations, we truncate the distributions at $N = 800$, and the distributions are therefore peaked at that value. If longer polymers are included, then the condensed MW distribution moves nearer to the maximum present chain length at the cloud point. These results emphasize that the shape and decay of the molecular distribution determine the fractionation behavior, particularly near the cloud point.

The results demonstrated in Fig. 2 are extracted at the cloud point at one value of χ . In Fig. S1, we demonstrate that fractionation is weaker as χ decreases since there is a lesser driving force for demixing, consistent across all distributions tested. Furthermore, as polymer is added to solution beyond the cloud point, eventually the dry and condensed-phase distributions become similar, as fractionation of low MW components into the dilute phase eventually dominates.

Since the MW distribution in the condensed phase differs from the overall MW distribution, one may ask: is the coexistence curve itself sensitive to the MW distribution? In Fig. 3, we explore this question at the cloud point for the distributions from Table 1 by calculating the coexistence curves, expressed as $\chi(\phi_t)$. Note that each point along the coexistence curve corresponds to a unique MW distribution in each phase, but the phase diagram is simplified by projecting all phase compositions onto the coordinate ϕ_t . In each plot, a thin dashed black line is plotted that matches the result if the polymer were purely monodisperse at the weight-average MW (Table 1).

Clearly, the larger the polydispersity of the sample, the greater the shift of the coexistence curve from what one would expect for a monodisperse sample. This trend is most clearly seen for the normally distributed samples in Fig. 3(a) with varying standard deviation. Further, the degree of shifting in the coexistence curve becomes more significant at larger values of χ , as the phase equilibrium becomes more dominated by the larger MW components. These shifts can be significant, considering that the ϕ_t axis is plotted with a logarithmic scale.

There is further sensitivity of the phase diagram as the volume fractions of the condensed phases change, as shown in Fig. S2.

There are also cases where the coexistence curve is less sensitive to the MW distribution. For example, the modified-Poisson distributed samples in Fig. 3(b) exhibit a weak shifting of the curve, which is only relevant at large χ . Regardless of the ratio between peaks, the bimodal distributions in Fig. 3(c) are dominated by the higher MW peak regardless of the ratio between the peak heights.

The largest deviations from the monodisperse behavior are found for the Flory-Schulz distribution in Fig. 3(d), which is consistent with the extreme fractionation in these distributions with longer tails. In these samples, there is a “notch” in the coexistence curve near the apparent critical point, which is not a numerical artefact and to our knowledge has not been mentioned before. The appearance of this notch is puzzling as it is a consequence of the projection of the phase diagram into the ϕ_t coordinate. The notch can be more clearly

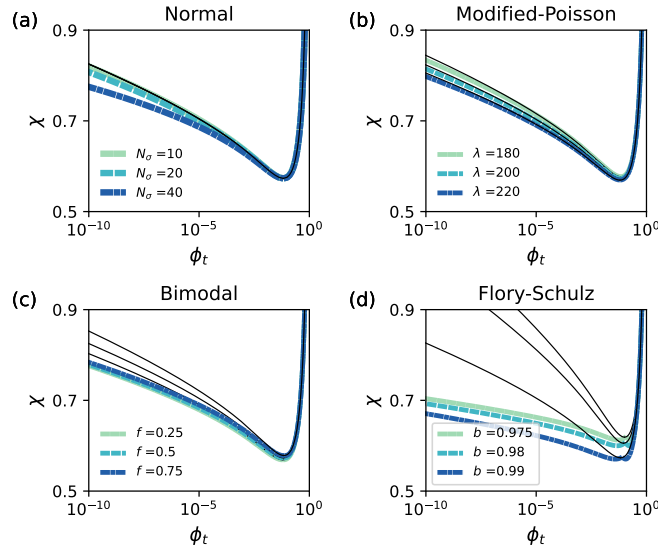


Figure 3: Polydispersity shifts the phase boundary. The two-phase coexistence curves are plotted as $\chi(\phi_t)$, evaluated at the cloud point where an infinitesimal amount of condensed phase is formed. The overall (dry) MW distributions are the same as in Fig. 2, with (a) a normally distributed polymer sample with varying standard deviation, (b) a modified-Poisson distributed sample, (c) a bimodal distributed polymer sample, and (d) a Flory-Schulz distributed sample with varying degrees of polymerization.

interpreted in the context of the overall phase diagram surface beyond the cloud point, the subject we turn to next.

Finally, we turn to the calculation of the overall phase diagram in Fig. 4. In Fig. 4(a), the overall phase diagram is projected to the surface $\chi(\phi_t, \bar{\phi})$, where ϕ_t corresponds to the total polymer volume fraction in each phase, ϕ_{tB} and ϕ_{tA} , and $\bar{\phi}$ corresponds to the overall volume fraction of polymer added to solvent. This surface plot embeds a lot of information, but it can be read as follows: (i) Draw a horizontal line corresponding to the overall volume fraction of polymer, $\bar{\phi}$. (ii) Find the intersection of the horizontal line with the corresponding value of χ on the left and right colored regions. The intersection in the left colored region gives the dilute phase ϕ_{tB} , while the intersection on the right colored region gives the condensed phase volume fraction ϕ_{tA} . The point where the two regions meet is the global critical point.

For monodisperse samples at fixed χ , the dilute and condensed phases have fixed composition regardless of the overall volume fraction of the polymer. Therefore, an ideal monodis-

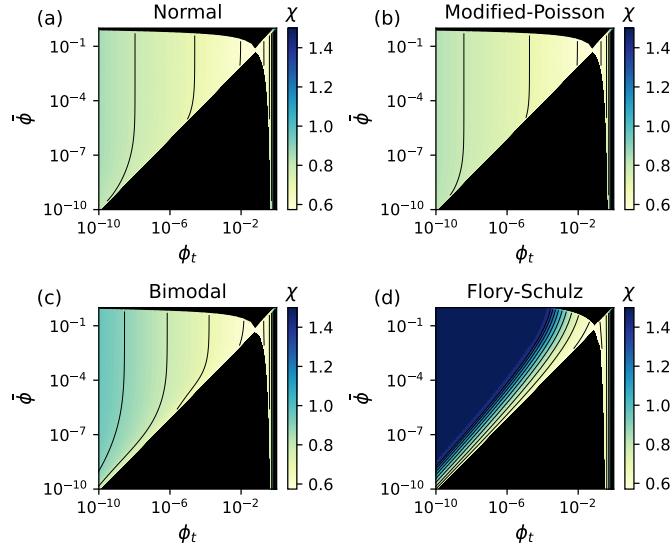


Figure 4: Full phase diagrams for different MW distributions. The overall phase diagram surface $\chi(\phi_t, \bar{\phi})$, where ϕ_t is the sum of all components in a given phase and $\bar{\phi}$ is the overall volume fraction of polymer added to the solution. The values are saturated at the bounds of the color bar. The samples are (a) a normally distributed sample with $\langle N \rangle = 200$ and $N_\sigma = 20$, (b) a modified Poisson sample with $\lambda = 200$, (c) a bimodal distribution with $f = 0.5$, and (d) a Flory-Schultz sample with $b = 0.99$.

perse sample would have contours on the χ surface that are nearly perfectly vertical, which is closely mirrored by the modified-Poisson sample displayed in Fig. 4(b). On the other hand, a shift in the bulk composition of the two phases with increasing overall polymer volume fraction corresponds to angled contours on the χ surface. The normally distributed sample exhibits some of this angled behavior in Fig. 4(a), which is comparatively more extreme for the bimodal and Flory-Schulz distributions in Fig. 4(c) and (d), respectively.

The Flory-Schulz distribution again exhibits the greatest deviation relative to monodisperse behavior. The χ -contours appear to be nearly at 45° on the dilute side of the $\chi(\phi_t, \bar{\phi})$ surface. As shown in Fig. S3, even the contours near the critical point are angled and intersect with the critical point for the Flory-Schulz distribution, which is not the case for other distributions. This unique feature is responsible for causing the apparent “notch” in the phase diagram near the apparent critical point in Fig. 3(d), even though this notch does not appear near the global critical point.

Each point on the phase diagram corresponds to a unique MW distribution in the condensed and dilute phases. If we follow the $\chi = 0.8$ contour on Fig. 4(a) as $\bar{\phi}$ is increased, we can directly evaluate how the MW distribution changes while increasing the overall polymer volume fraction. In the SI Fig. S4, the MW distribution is plotted as $p(N; \bar{\phi})$ for the dilute and condensed phases, respectively. As the polymer volume fraction is increased, the condensed phase (Phase A) distribution eventually matches the overall molecular weight distribution. Conversely, the dilute phase (Phase B) distribution goes from matching the overall distribution to selecting for shorter molecular weight components as $\bar{\phi}$ increases.

In summary, by direct evaluation of analytical formulas of polymer fractionation, we have shown that the shape of the MW distribution is crucial in phase coexistence calculations. The greater the polydispersity, the greater the fractionation of MWs between phases and the shift of the coexistence curve relative to monodisperse samples. The tail of the MW distribution dominates in the phase coexistence calculations, especially for distributions with long tails or for bimodal distributions near their cloud point.

In our analysis, we have performed all calculations in terms of χ , but the exact value of χ may depend on temperature and the solvent identity. The calculations are done assuming that all polymers have the same monomer composition, and future work could extend the analysis to copolymer systems with polydispersity in size and chemical composition.^{26,27} Further, while the calculations done here correspond to a *batch* process in which there are no spatial gradients or temporal evolution in composition, fractionation processes may be designed in which the overall MW distribution (and in each phase) may become a function of space and time.³

The analytical approach explored here may be extended to such scenarios where model-based simulation and optimization would be aided by efficient phase coexistence calculations. The approach allows for the computationally-efficient consideration of the entire MW distribution at high numerical accuracy, providing a method to describe the essential role of polydispersity in polymeric phase separation.

Acknowledgement

JPD and HAS acknowledge support from the Princeton Center for Complex Materials, an NSF MRSEC (DMR-2011750), and NSF for grant DMS/NIGMS 2245850. JPD is also supported by the Omenn-Darling Princeton Bioengineering Institute – Innovators (PBI2) Postdoctoral Fellowship. WMJ acknowledges support from the National Institute of General Medical Sciences of the National Institutes of Health under award number R35GM155017.

Supporting Information Available

Detailed description of fractionation calculations, discussion of previous fractionation calculation approaches, and supplementary plots characterizing phase diagrams.

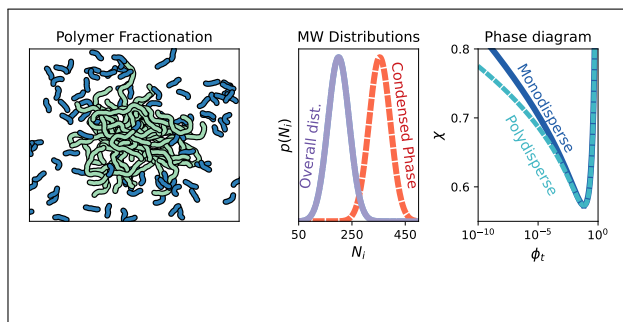
References

- (1) Flory, P. J. *Principles of Polymer Chemistry*; Cornell University Press, 1953.
- (2) Cantow, M. J. *Polymer Fractionation*; Academic Press Inc, 1967.
- (3) Francuskiewicz, F. *Polymer Fractionation*; Springer Science & Business Media, 2013.
- (4) Hiemenz, P. C.; Lodge, T. P. *Polymer Chemistry*; CRC Press, 2007.
- (5) Gentekos, D. T.; Sifri, R. J.; Fors, B. P. Controlling polymer properties through the shape of the molecular-weight distribution. *Nature Reviews Materials* **2019**, *4*, 761–774.
- (6) Odian, G. *Principles of Polymerization*; John Wiley & Sons, 2004.
- (7) Billmeyer Jr., F. W. Characterization of molecular weight distributions in high polymers. *Journal of Polymer Science Part C: Polymer Symposia* **1965**, *8*, 161–178.
- (8) Whitfield, R.; Truong, N. P.; Messmer, D.; Parkatzidis, K.; Rolland, M.; Anastasaki, A. Tailoring polymer dispersity and shape of molecular weight distributions: methods and applications. *Chemical Science* **2019**, *10*, 8724–8734.
- (9) Mencer, H. Efficiency of polymer fractionation—A review. *Polymer Engineering & Science* **1988**, *28*, 497–505.
- (10) Wang, T.-T.; Luo, Z.-H.; Zhou, Y.-N. On the Precise Determination of Molar Mass and Dispersity in Controlled Chain-Growth Polymerization: A Distribution Function-Based Strategy. *Macromolecules* **2023**, *56*, 1130–1140.
- (11) Ward, I. M.; Sweeney, J. *Mechanical Properties of Solid Polymers*; John Wiley & Sons, 2012.
- (12) Bird, R. B.; Armstrong, R. C.; Hassager, O. *Dynamics of Polymeric Liquids. Vol. 1: Fluid Mechanics*; John Wiley and Sons Inc., New York, NY, 1987.

- (13) Godovsky, Y. K. *Thermophysical Properties of Polymers*; Springer Science & Business Media, 2012.
- (14) Ward, M. A.; Georgiou, T. K. Thermoresponsive polymers for biomedical applications. *Polymers* **2011**, *3*, 1215–1242.
- (15) Blythe, A. R.; Bloor, D. *Electrical Properties of Polymers*; Cambridge University Press, 2005.
- (16) Higashihara, T.; Ueda, M. Recent progress in high refractive index polymers. *Macromolecules* **2015**, *48*, 1915–1929.
- (17) Shin, Y.; Brangwynne, C. P. Liquid phase condensation in cell physiology and disease. *Science* **2017**, *357*, eaaf4382.
- (18) Banani, S. F.; Lee, H. O.; Hyman, A. A.; Rosen, M. K. Biomolecular condensates: organizers of cellular biochemistry. *Nature Reviews Molecular Cell Biology* **2017**, *18*, 285–298.
- (19) Jacobs, W. M. Theory and simulation of multiphase coexistence in biomolecular mixtures. *Journal of Chemical Theory and Computation* **2023**, *19*, 3429–3445.
- (20) Tian, S.; Curnutte, H. A.; Trcek, T. RNA granules: a view from the RNA perspective. *Molecules* **2020**, *25*, 3130.
- (21) Heidemann, R. A.; Michelsen, M. L. Instability of successive substitution. *Industrial & Engineering Chemistry Research* **1995**, *34*, 958–966.
- (22) van Leuken, S. H.; van Benthem, R. A.; Tuinier, R.; Vis, M. Predicting Multi-Component Phase Equilibria of Polymers using Approximations to Flory–Huggins Theory. *Macromolecular Theory and Simulations* **2023**, *32*, 2300001.

- (23) de Souza, J. P.; Stone, H. A. Exact analytical solution of the Flory–Huggins model and extensions to multicomponent systems. *The Journal of Chemical Physics* **2024**, *161*, 044902.
- (24) Huggins, M. L.; Okamoto, H. *Polymer Fractionation*; Elsevier, 1967; pp 1–42.
- (25) Note that distributions of this type may be reasonably approximated by a normal distribution when λ is large.
- (26) van Leuken, S. H. M.; van Osch, D. J. G. P.; Kouris, P. D.; Yao, Y.; Jedrzejczyk, M. A.; Cremers, G. J. W.; Bernaerts, K. V.; van Benthem, R. A. T. M.; Tunier, R.; Boot, M. D.; Hensen, E. J. M.; Vis, M. Quantitative prediction of the solvent fractionation of lignin. *Green Chem.* **2023**, *25*, 7534–7540.
- (27) Chen, F.; Jacobs, W. M. Emergence of multiphase condensates from a limited set of chemical building blocks. *Journal of Chemical Theory and Computation* **2023**,

TOC Graphic



Supplementary information: Polydisperse polymer fractionation between phases

J. Pedro de Souza,^{*,†} William M. Jacobs,^{*,‡} and Howard A. Stone^{*,¶}

[†]*Omenn-Darling Bioengineering Institute, Princeton University, Princeton, NJ, 08544*

[‡]*Department of Chemistry, Princeton University, Princeton, NJ 08544, USA.*

[¶]*Department of Mechanical and Aerospace Engineering, Princeton University, Princeton, NJ, 08544*

E-mail: pdesouza@princeton.edu; wjacobs@princeton.edu; hastone@princeton.edu

S1 Previous fractionation calculation approach

Flory[?] and Huggins[?] each found that the chemical equilibrium, by equating $\mu_i - \Pi$ (in our notation), provides a relationship describing the fractionation of each polymeric component,

$$\frac{\phi_{iA}}{\phi_{iB}} = \exp(N_i \Omega), \quad (\text{S1})$$

with the function Ω defined as

$$\Omega = (-1 + 2\chi)(\phi_{At} - \phi_{Bt}) - \chi(\phi_{At}^2 - \phi_{Bt}^2) + \sum_i \frac{\phi_{iA} - \phi_{iB}}{N_i}. \quad (\text{S2})$$

Both authors treated Ω as an effective fitted constant, and did not attempt to solve the fractionation problem exactly. Combined with a mass balance of polymer species i , the above

treatment gives an exact formula for the fraction of polymer i in the concentrated phase, θ_i :

$$\theta_i = \frac{\nu\phi_{iA}}{\nu\phi_{iA} + (1 - \nu)\phi_{iB}} = \frac{\nu e^{N_i\Omega}}{1 - \nu + \nu e^{N_i\Omega}} \quad (\text{S3})$$

where ν is the volume fraction of the condensed phase.

While this mathematical treatment gives helpful information on the separation of polymers between phases, it does not answer how the polydispersity of polymers themselves alter the phase diagram in terms of χ . The value of Ω , which is in principle a function of the concentrations of all species in both phases, must be fitted to an experimental data set at each particular condition. Further, the value of Ω may be sensitive to the volume of the condensed phase. This means that the above expression can be used to interpret fractionation data, but is not systematically transferable between different experimental conditions.

S2 Exact analytical solution implementation

To solve the thermodynamic calculation exactly for a polydisperse sample with the allowable degrees of freedom, we recently proposed an implicit substitution method that makes use of composite composition variables.[?] We include details of the fractionation calculation below, and refer to [?] for details on the derivation.

Here, we will specify the component of index 1 to be the component closest to the mass average molecular weight of the overall polymer sample. To start, we frame the equations in terms of a differential partitioning variable, y_i , between the two phases, defined as

$$y_i = \frac{\phi_{iA} - \phi_{iB}}{\phi_{iA} + \phi_{iB}}. \quad (\text{S4})$$

y_i is a measure of the partitioning of component i and can also indicate the distance from

the critical point. By setting $\mu_i - \mu_1$ equal to each other in each phase, we find

$$y_i = \tanh \left(\frac{N_i}{N_1} \tanh^{-1}(y_1) \right). \quad (\text{S5})$$

Next, by solving each chemical potential equilibrium equation for χ , and then subtract a linear combination of them from the value of χ from the osmotic pressure equation, we can solve for all the densities exactly. In order to do so, we reframe the equations in terms of the solvent partitioning, z ,

$$z = \frac{\phi_{tA} - \phi_{tB}}{2 - \phi_{tA} - \phi_{tB}} \quad (\text{S6})$$

and the set of relative partitioning variables, w_i ,

$$w_i = \frac{\phi_{iA} - \phi_{iB}}{\phi_{1A} - \phi_{1B}}, \quad (\text{S7})$$

comparing the partitioning of component i to component 1. Here, we will independently set two variables, (i) the partitioning of component 1, y_1 , and (ii) the volume fraction of the condensed phase, ν . These are two independent degrees of freedom that will specify the entire two-phase diagram.

From the mass balance for each component,

$$\bar{\phi} = \nu \phi_{iA} + (1 - \nu) \phi_{iB} \quad (\text{S8})$$

and the mass balance of component 1, we can define w_i in terms of ν and y_1 ,

$$w_i = \frac{p(N_i)}{p(N_1)} \frac{\left(\nu + \frac{1}{2y_1} - \frac{1}{2} \right)}{\left(\nu + \frac{1}{2y_i} - \frac{1}{2} \right)}, \quad (\text{S9})$$

where $p(N_i)$ is the known probability density of component i in the “dry” polymer sample without solvent.

We can now account for the number of equations and unknown composite variables we

must solve for. There are $M - 1$ equations describing the set w_i in S9. The equilibrium constraints on each component's chemical potential and osmotic pressure give $M + 1$ equations, for a total of $2M$ equations. In terms of the composite variables, the unknowns are the M values of y_i , the $M - 1$ values of w_i (since $w_1 = 1$ automatically), as well as z , ν , and χ , for a total of $2M + 2$ unknowns. Therefore, we have two degrees of freedom, which we use to independently specify y_1 and ν over their allowable range, then find all other composite variables.

By setting y_1 and ν and having knowledge of the overall molecular weight distribution $p(N_i)$, we can find z exactly by enforcing osmotic equilibrium:

$$z = h^{-1} \left(1 + \frac{\sum_i w_i (h(y_i) - 1)/N_i}{\sum_i w_i} \right), \quad (\text{S10})$$

where we have defined the Flory-Huggins (FH) function $h()$ as

$$h(x) = \frac{\tanh^{-1}(x)}{x}. \quad (\text{S11})$$

Its inverse, $h^{-1}()$, can be efficiently computed by lookup tables or by a series representation, which is derived in Section S4 of the SI.

Finally, equipped with the value of z , we can map the composite composition coordinates back to real composition space,

$$\{y_i, z, w_i, \nu\} \rightarrow \{\phi_{iA}, \phi_{iB}, \chi\}. \quad (\text{S12})$$

Explicitly, the mappings take the form

$$\phi_{iA} = \frac{1}{2}\beta_i(1 + y_i) \quad (\text{S13a})$$

$$\phi_{iB} = \frac{1}{2}\beta_i(1 - y_i) \quad (\text{S13b})$$

and

$$\chi = \frac{2 \tanh^{-1}(z) + \sum_i \left(\frac{1}{N_i} - 1 \right) \beta_i y_i}{\gamma_0}. \quad (\text{S14})$$

For the polydisperse sample, the constants γ_0 and β_i are defined as

$$\gamma_0 = \sum_i \sum_j (\phi_{iA} \phi_{jA} - \phi_{iB} \phi_{jB}) \quad (\text{S15})$$

and

$$\beta_i = \frac{2zw_i}{y_i \sum_j \left[w_j \left(1 + \frac{z}{y_j} \right) \right]}. \quad (\text{S16})$$

For the polydisperse system under study, one may notice that all the real composition variables can be computed based on three weighted sums of the molecular weight distribution for a fixed y_1 and ν . These weighted sums can be expressed as I_k ($k = 1, 2, 3$):

$$I_k = \sum_{N_i=1}^{N_i=N_{\max}} \frac{p(N_i)}{p(N_1)} Q_k(N_i). \quad (\text{S17})$$

The weighting functions $Q_k(N_i)$ are defined as

$$Q_1(N_i) = \frac{\nu + \frac{1}{2y_1} - \frac{1}{2}}{\nu + \frac{1}{2y(N_i)} - \frac{1}{2}} \quad (\text{S18a})$$

$$Q_2(N_i) = Q_1(N_i) \frac{h(y(N_i)) - 1}{N_i} \quad (\text{S18b})$$

$$Q_3(N_i) = \frac{Q_1(N_i)}{y(N_i)}. \quad (\text{S18c})$$

Recasting the computed variables in terms of these weighted sums, the volume fraction in the condensed phase (A) for each species is

$$\phi_A(N_i) = \frac{zp(N_i)Q_1(N_i)(1 + y(N_i))}{p(N_1)y(N_i)(I_1 + zI_3)}, \quad (\text{S19})$$

and in the dilute phase (B) the volume fraction is

$$\phi_B(N_i) = \frac{zp(N_i)Q_1(N_i)(1 - y(N_i))}{p(N_1)y(N_i)(I_1 + zI_3)}. \quad (\text{S20})$$

The partitioning of the solvent, z , can be written in form

$$z = h^{-1} \left(1 + \frac{I_2}{I_1} \right). \quad (\text{S21})$$

The total polymer volume fractions in each phase are then

$$\phi_{tA} = \frac{z(I_3 + I_1)}{I_1 + zI_3} \quad (\text{S22a})$$

$$\phi_{tB} = \frac{z(I_3 - I_1)}{I_1 + zI_3}, \quad (\text{S22b})$$

and the total polymer volume fraction, $\bar{\phi}$ in the solution can be computed as

$$\bar{\phi} = \nu\phi_{tA} + (1 - \nu)\phi_{tB}. \quad (\text{S23})$$

Therefore, to generate plots with $\bar{\phi}$ as a coordinate, we vary ν between 0 and 1, then map to $\bar{\phi}$.

S3 Fractionation at the tails of the distribution at the cloud point

Here, we will analyze fractionation at the tails of the distribution far from the critical point, but located at the cloud point, $\nu = 0$. In this limit, we can safely assume that $y(N_i) \approx 1 - \epsilon(N_i)$ where $\epsilon(N_i) \ll 1$. In this limit, using equation S5, we get

$$\epsilon(N_i) = 2 \left(\frac{\epsilon_1}{2} \right)^{N_i/N_1}. \quad (\text{S24})$$

The volume fraction of component with length N_i relative to the mass average length, N_1 , in the condensed phase is defined by the ratio

$$\frac{\phi_A(N_i)}{\phi_A(N_1)} = \frac{\beta(N_i)(1 + y(N_i))}{\beta(N_1)(1 + y(N_1))} \approx w(N_i) \quad (\text{S25})$$

with $w(N_1) = 1$. At the cloud point, $\nu = 0$, with equation S9, we can relate $w(N_i)$ to ϵ_1 ,

$$\frac{\phi_A(N_i)}{\phi_A(N_1)} \approx \frac{p(N_i)}{p(N_1)} \left(\frac{\epsilon_1}{2} \right)^{1-N_i/N_1} \quad (\text{S26})$$

Equation S26 highlights the asymptotic behavior far from the critical point but also at the cloud point. If the MW distribution decays more slowly than exponential, then the highest molecular weight species will dominate the condensed phase, as was seen for the Flory-Schulz MW distribution.

By evaluating the weighting functions in this limit, we can determine the limiting molecular weight distribution far from the critical point. The weighting functions take on the limiting forms

$$Q_1(N_i) = \left(\frac{\epsilon_1}{2} \right)^{1-N_i/N_1} \quad (\text{S27a})$$

$$Q_2(N_i) \approx \left(-\frac{1}{2N_1} \ln(\epsilon_1/2) - \frac{1}{N} \right) Q_1(N_i), \quad (\text{S27b})$$

$$Q_3(N_i) \approx (1 + 2(\epsilon_1/2)^{N/N_1}) Q_1(N_i) \quad (\text{S27c})$$

and the partitioning of each component is

$$y(N_i) \approx 1 - 2(\epsilon_1/2)^{N/N_1}. \quad (\text{S27d})$$

In terms of the N_i dependence of the distribution, we find the following relationship far from the critical point for the condensed and dilute phases, respectively,

$$\phi_A(N_i) \propto p(N_i) \left(\frac{\epsilon_1}{2} \right)^{1-N_i/N_1} \quad (\text{S28a})$$

$$\phi_B(N_i) \propto p(N_i)\epsilon_1. \quad (\text{S28b})$$

S4 Inverse FH function calculation

Here, we pursue a series representation of the inverse FH-function, which is related to the Generalized-LambertW function. The FH equation has the form

$$h(z) = \frac{\tanh^{-1}(z)}{z} = \frac{1}{2z} \ln \left(\frac{1+z}{1-z} \right) = A, \quad (\text{S29})$$

First, we define the variable $x = -2zA$, so that the equation takes the convenient form

$$2A - x = (2A + x) e^{-x}. \quad (\text{S30})$$

Or in other terms:

$$x = -2A + (2A - x)e^x \quad (\text{S31})$$

Using the Lagrange reversion theorem, the solution for x can be described by:

$$x = -2A + \sum_{k=1}^{\infty} \frac{1}{k!} \left(\frac{d}{dx} \right)^{k-1} \left[(2A - x)^k e^{kx} \right]_{x=-2A}. \quad (\text{S32})$$

We can then define $u = -kx + 2Ak$

$$x = -2A + \sum_{k=1}^{\infty} \frac{(-k)^{k-1}}{k!} \left(\frac{d}{du} \right)^{k-1} \left[\left(\frac{u}{k} \right)^k e^{-u+2Ak} \right]_{u=4Ak} \quad (\text{S33})$$

and reformulate as:

$$x = -2A - \sum_{k=1}^{\infty} \frac{(-1)^k}{k!k} e^{2Ak} \left(\frac{d}{du} \right)^{k-1} \left[u^k e^{-u} \right]_{u=4Ak}. \quad (\text{S34})$$

Next, we make use of the following identity

$$\left(\frac{d}{du}\right)^{k-1} [u^k e^{-u}] = (k-1)! u e^{-u} L_{k-1}^{(1)}(u) \quad (\text{S35})$$

where $L()$ signifies the generalized Laguerre polynomials, so that we can write the final inversion formula as

$$x = -2A - \sum_{k=1}^{\infty} \frac{4A(-1)^k}{k} e^{-2Ak} L_{k-1}^{(1)}(4Ak). \quad (\text{S36})$$

Or in terms of z , we get:

$$z = 1 + 2 \sum_{k=1}^{\infty} \frac{(-1)^k}{k} e^{-2Ak} L_{k-1}^{(1)}(4Ak). \quad (\text{S37})$$

The series converges well for intermediate values of $1.076 < A < 5$, which we can confirm by evaluating 100 terms in the series. To maintain accuracy outside of these bounds (since A can vary between 1 and ∞), we apply asymptotic solutions for A in the limit of large and small A . For $A < 1.076$, we expand up to sixth order and truncate,

$$h(z) \approx 1 + \frac{z^2}{3} + \frac{z^4}{5} + \frac{z^6}{7} = A, \quad (\text{S38})$$

then solve a cubic equation for z^2 , keeping the real, positive root of z .

For $A > 5$, we use the limiting formula:

$$h(z) \approx \frac{1}{2} \ln \left(\frac{2}{1-z} \right) = A \quad (\text{S39})$$

from which we can derive:

$$z = 1 - 2e^{-2A}, \quad (\text{S40})$$

valid at large values of A .

Using these series and asymptotic expressions, the maximum error for

$$h\left(h^{-1}(A)\right) \tag{S41}$$

is within 0.02% of A over the entire possible range of A .

S5 Supplementary results

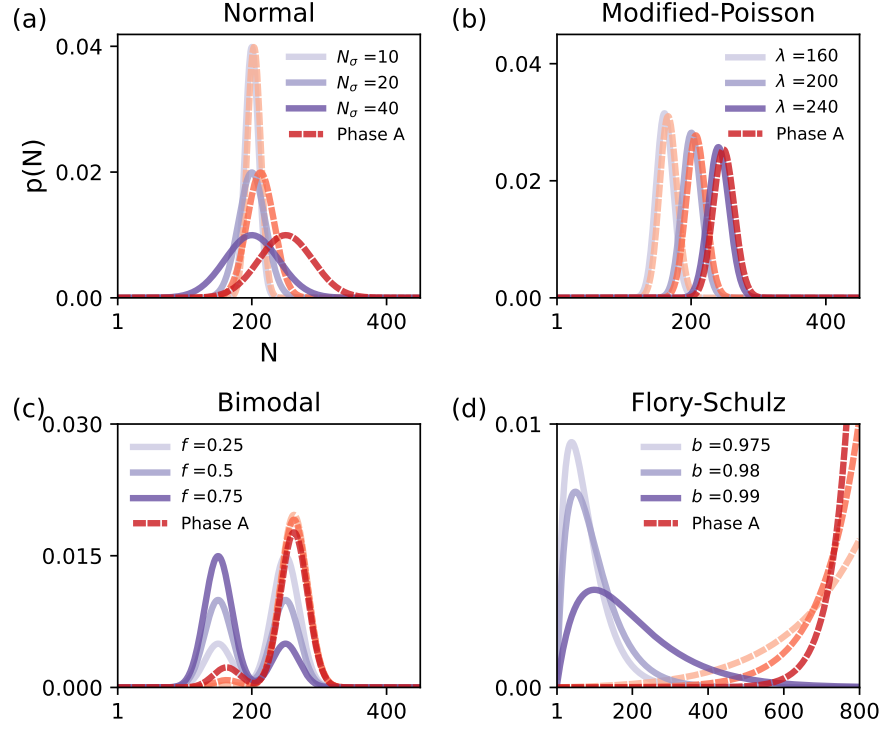


Figure S1: Phase coexistence at a different value of χ . The same distributions as those in Figure 2 in the main text are used, but the condensed phase (Phase A) distributions are evaluated at $\chi = 0.65$ instead of $\chi = 0.8$. The degree of fractionation changes based on the value of χ .

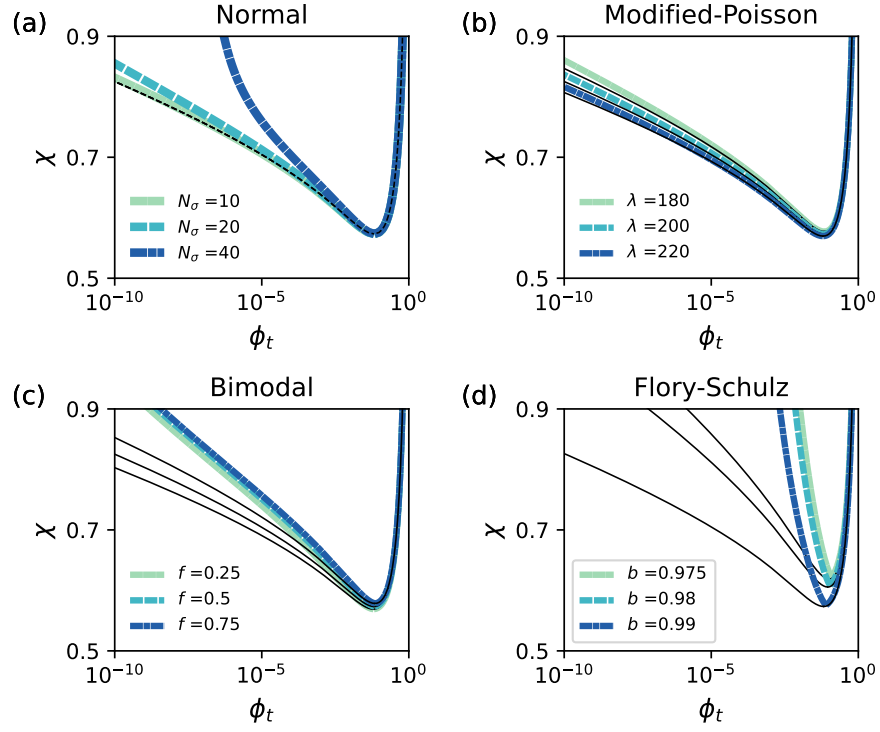


Figure S2: Phase diagrams evaluated at high condensed phase volume fraction ($\nu = 1$). The same overall distributions are used as in the main text Figure 3. The more polydisperse samples exhibit a greater sensitivity in their phase diagram to changing the condensed volume fraction.

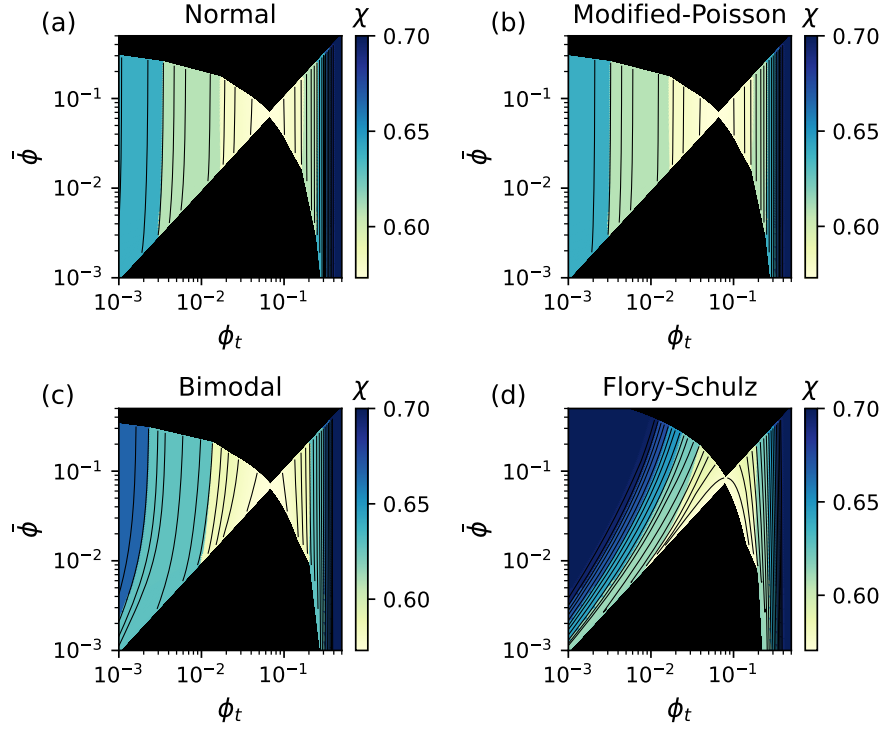


Figure S3: Zooming into the critical point for the overall phase diagram. The Flory-Schulz model exhibits a unique feature at its critical point, where a single χ contour appears to traverse the critical point. The other distributions do not share this feature.

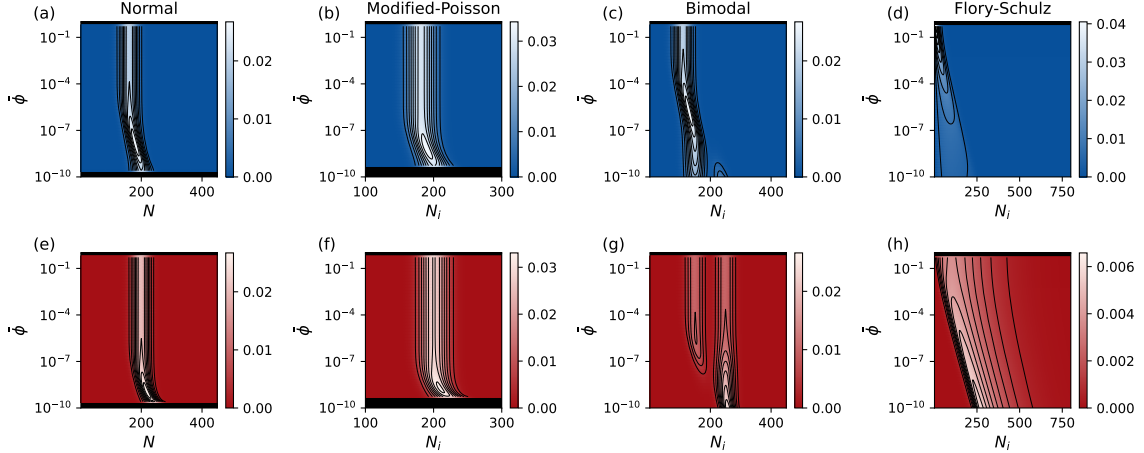


Figure S4: The molecular weight distributions plotted as a function of the overall polymer volume fraction at a fixed value of $\chi = 0.8$, corresponding to the phase diagrams in Figure 4 in the main text. The top row corresponds to the dilute phase, while the bottom row corresponds to the concentrated phase. (a,e) correspond to the normally distributed sample, (b,f) correspond to the modified -Poisson distributed sample, (c,g) correspond to the bimodal distributed sample, and (d,h) correspond to the Flory-Schulz distributed sample.